Electronic Supplementary Material (ESI) for Lab on a Chip.
This journal is © The Royal Society of Chemistry 2017

Open Channel Deterministic Lateral Displacement for Particle and Cell Sorting

Trung S.H. Tran, Bao D. Ho, Jason P. Beech and Jonas O. Tegenfeldt

Electronic Supporting Information

Design and fabrication

The basic operational principle of DLD along with relevant parameters and critical separation diameters for our DLD devices are shown in Figure S1.

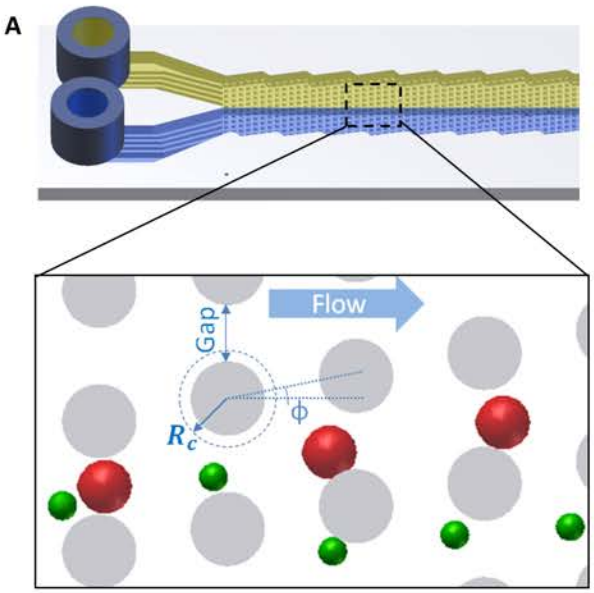

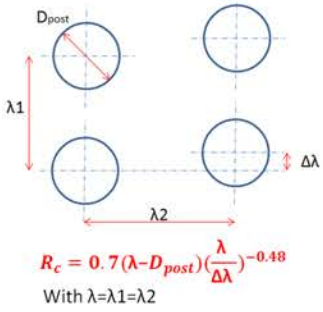

C

Device	Dpost	Gap	Dc	Depth
1	30	11	5.1	24
2	30	23	10.7	24
3	30	31	14.4	24
4	20	12	5	24
5	20	12	5	9

Figure S1*. (A) Schematic of a typical DLD device with particle trajectories, (B) Key parameters determining the critical diameter (D_c) of a DLD array, (C) List of DLD devices used in this report (length units are µm). Length of the devices is 20 mm and width is 4 mm.*

Several fabrication and surface treatment schemes were tested for our devices (Figure S2). Figure S2A shows the conventional method of fabricating closed PDMS/glass devices with a plasma-bonding step (that also renders the PDMS hydrophilic) and the attachment of reservoirs/pressure control connections.

Preparation of devices

For the open devices, if a drop of aqueous solution is applied at the end of an untreated (hydrophobic) DLD array, the droplet will stay on the surface and will not wet the channels or array area of the device. This can be overcome in two ways. Figure S2B shows an open device in which the channels are selectively rendered hydrophilic by use of a mask during oxygen plasma treatment. The untreated, hydrophobic PDMS surrounding the active area of the device serves to confine the sample, which would otherwise spread outside the features of the device. Another approach, that is simpler because oxygen plasma is not needed, is

shown in Figures S2C and D. By submerging the device in an aqueous solution (1% SDS for polystyrene bead sorting, AutoMacs™ for RBC, and complete Dulbecco's Modified Eagle's Medium (DMEM) for cancer cell experiments) at room temperature for 5 minutes, the entire surface of the device can be forced to wet. When the device is removed from the solution the flat PDMS surface is sufficiently hydrophobic to repel the aqueous solution, but the water inside the structures of the device remains. After the positioning of the paper capillary pump at the outlet and the addition of more sample at the inlet, flow is maintained and separation can be performed. The reservoir, shown in Figure S2D, is not essential but allows for greater control of the sample and the handling of larger sample volumes.

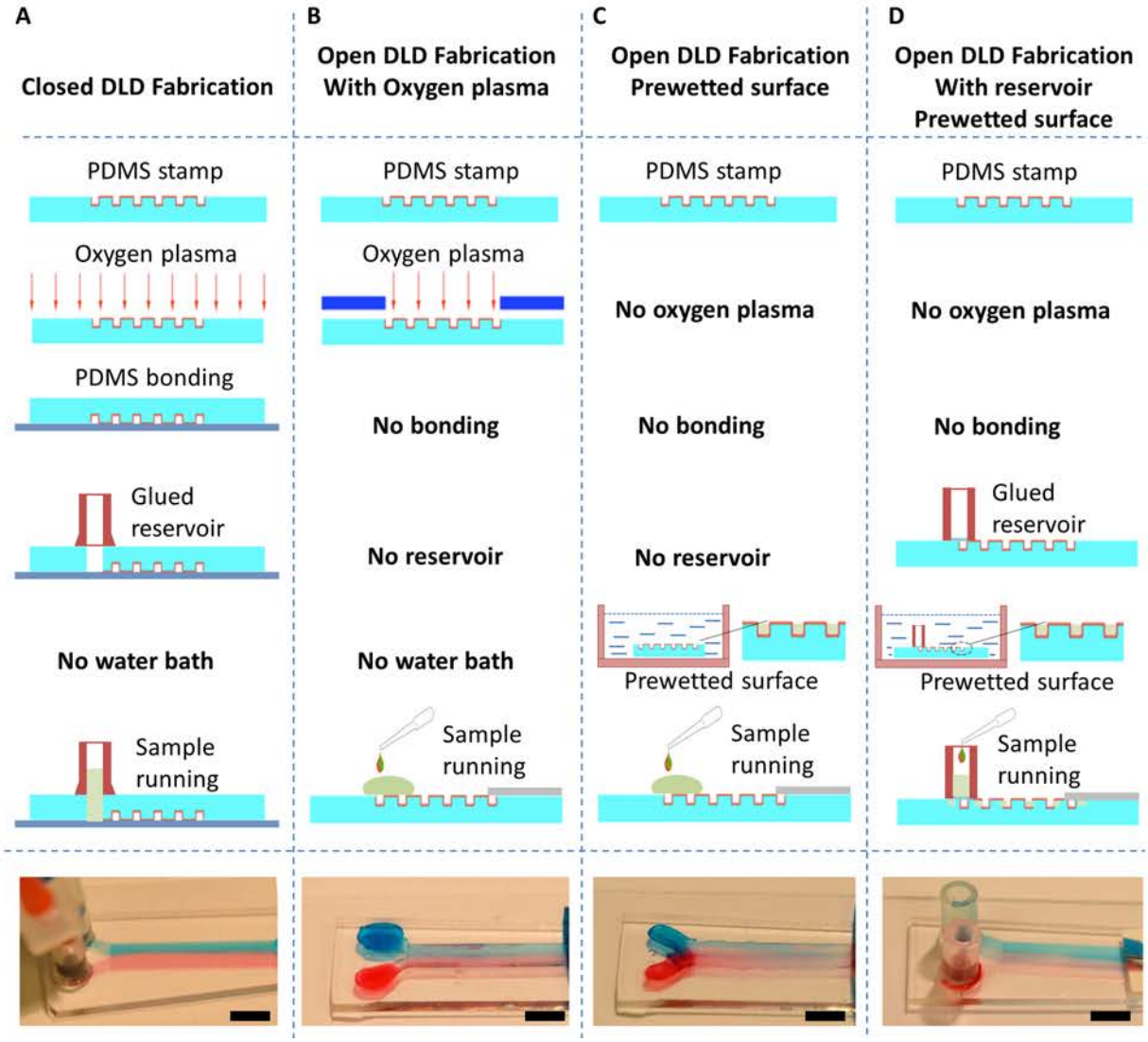

***Figure S2**. Comparison of different fabrication methods for closed and open DLD devices. (A) Conventional closed device fabrication. (B) Open device where the sorting structures are selectively treated with oxygen plasma to make them hydrophilic. (C) Rendering the PDMS hydrophilic by immersion (prewetting) in a water bath (plain water at room temperature in 5 minutes) instead of in an oxygen plasma. (D) Addition of a reservoir gives better control of the sample and allows for larger volumes. Scale bars 5 mm.*

The wetting of the devices using the different surface treatment strategies was characterized in more detail as presented in Figure S3. Selective oxygen plasma treatment gives a strongly hydrophilic surface with contact angle ~ 0°. Immersing the device in aqueous buffer gives a less hydrophilic surface (contact angle ~ 60° outside the device and an effective contact angle ~ 0° in the DLD array). The latter approach is fully adequate for the operation of the device and much simpler as it does not require any oxygen plasma equipment.

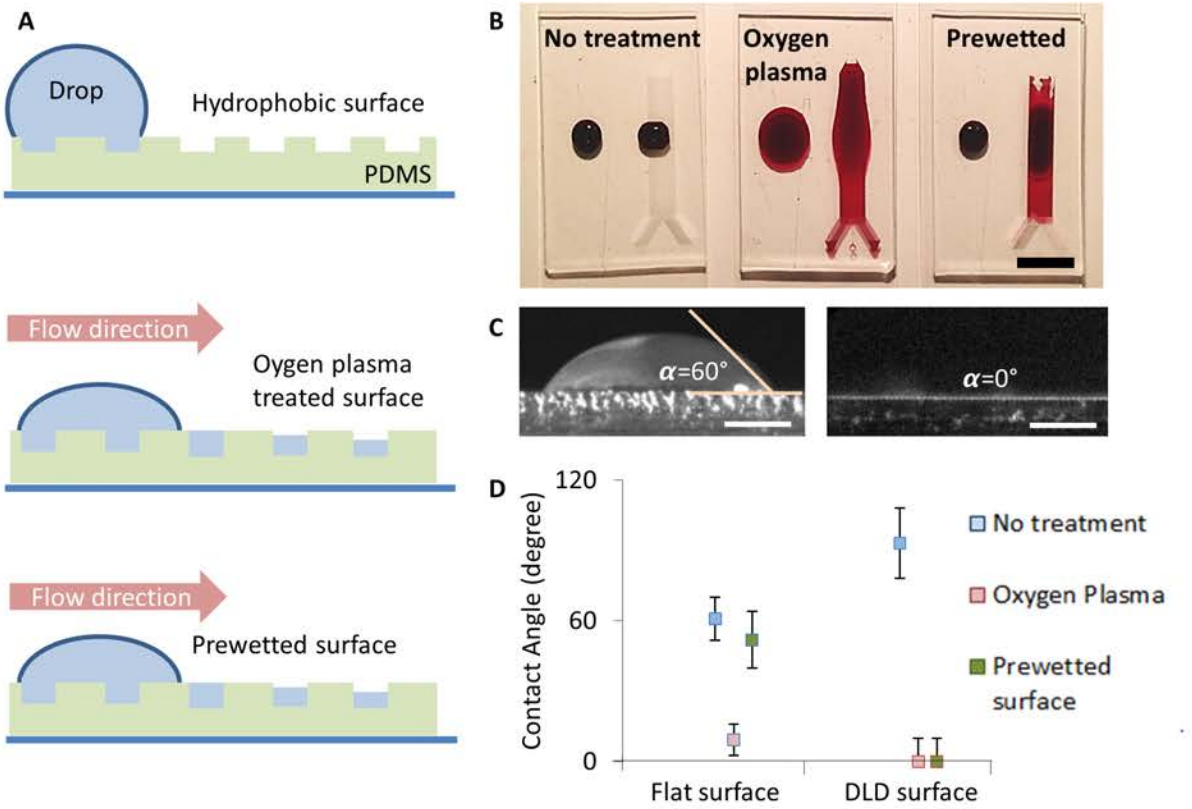

***Figure S3**. Hydrophobic and hydrophilic devices. (A) Schematic of a water droplet on an untreated (hydrophobic) surface and the two treated hydrophilic surfaces (B) Visualization of the wetting behavior of the three kinds of surface treatments on flat and patterned PDMS using an aqueous solution of red food coloring. (C) Cross-sectional view of water drop outside and on the DLD array for a prewetted surface. (D) Comparison of wetting angles on flat and patterned surfaces after no treatment, oxygen plasma and prewetting. The error bars represent the standard deviation of the measurement.*

Volume of a filled device

The volume of the liquid in a filled device is calculated based on the table in figure S1C. The ratio of the area of the fluid and the total area of the unit cell is 0.58, which is multiplied with the overall dimensions of the device (length 20 mm, width 4 mm and depth 24 µm), giving us the total volume of device 1 of 1.1 µL.

Uniformity of wetting

The characteristics and uniformity of the wetted array are characterized by confocal microscopy and direct imaging with a macro objective. In both cases device 3 was used with added reservoirs. For the confocal images fluorescein isothiocyanate (FITC) was first dissolved in methanol to 10% that was in turn diluted in water 100 times and the methanol

allowed to evaporate. The confocal microscope is based on a Yokogawa CSU22 spinning disc, Andor laser combiner and Andor iXon DU-897 CCD camera on an inverted Nikon Ti microscope. A Plan 50x ELWD Dry and a Plan Fluor ELWD 40x Ph2 ADL objective with NA 0.32 and 0.4 respectively where used for figures 2C-F. Since the microscope is inverted, the device was turned upside-down for imaging (surface tension dominates and so this has little to no effect on the shape of the liquid surface). The image contrast was adjusted such that scattered light was rejected from the image.

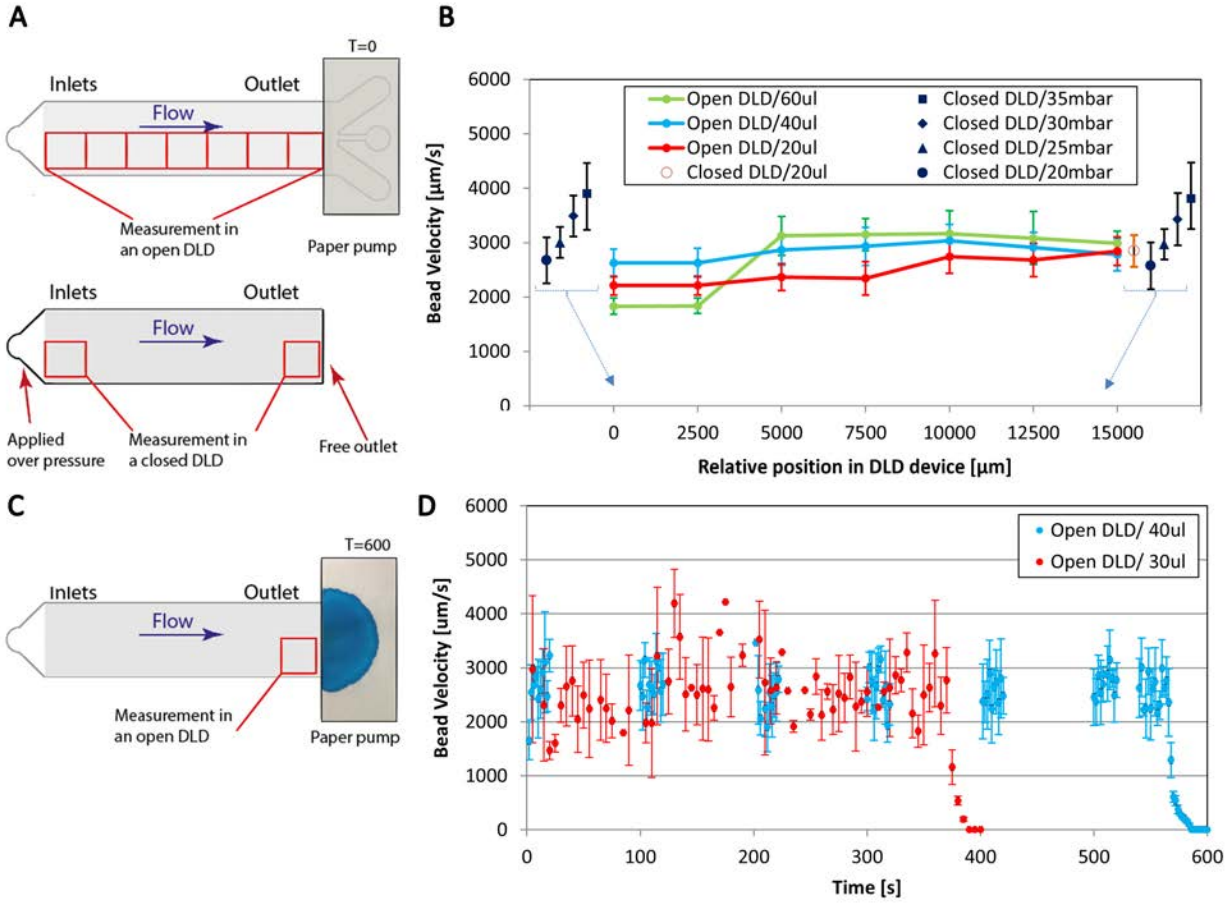

Figure S4. *Particle velocity measurements for open and closed DLD devices. The flow in the open devices is driven by a paper capillary pump without any wax-defined channels. The paper is shown at t=0 s in (A) and t=600 s in (C). The flow in the closed devices is driven by over pressure as well as by a paper capillary pump. The different sets of experiments took place using the same design of DLD (Device 1 (Figure S1)). The following microspheres were used at a dilution of 50x in deionized water: green fluorescent polystyrene beads with diameter 1.57 µm (CV 2%) and functionalized with carboxylate groups from Polysciences Inc. (Warrington, PA). (A) Schematic of measurement setup for velocity measurements at different locations for open and closed devices. (B) Velocity of the beads as a function of position for open and closed devices. For the data where a paper capillary pump was used the volume in the reservoir is indicated. For the pressure driven flow the applied pressure difference is given. (C) Schematic of measurement setup for velocity measurements as a function of time. (D) Velocity of beads as a function of time when 30 µL (red) and 40 µL (blue) of sample is added to the reservoir. The error bars represent the standard deviations of the measurements.*

For the images with the macro objective, the device is wetted with an aqueous food dye and imaged, with the liquid facing upwards, using a macro objective (Canon MP-E 65 mm f/2.8 1-5x) with a Canon 5D Mark II camera house. Basic contrast and brightness adjustments were made to ensure that the image reflects what is seen by the naked eye.

We could observe a tendency that the flow velocity (see below) is slightly lower for the first ~5 mm along the device. This indicates that the flow cross section is larger here, which is consistent with the flow extending above the posts since the volume flow rate is a conserved quantity. We observed that this effect vanishes as the fluid level drops, away from the reservoir and also decreases as the sample volume in the reservoir decreases with time.

Flow measurements

We measured the flow rates at different positions along open and closed devices using an applied overpressure or using a paper capillary pump (Figure S4). Velocities of fluorescent microspheres were observed between two neighboring posts in the same row.

The volumetric flow rates were measured directly by running the device with reservoirs filled with well-defined volumes and recording the elapsed time until the reservoirs were empty (Figure S4D). The volumes were corrected by subtracting the evaporated volume from the device based on figure S5 (8.5 nL/s). The time was measured until the velocity was half of the mean velocity. The remaining liquid in the device was crudely estimated to half the volume of the device, i.e. 0.5*1.1 µL. This volume was subtracted from the total volume considered. From these two measurements we obtain approximate values of 70 nL/s and 61 nL/s for the two different volumes tested. These results are consistent with the results of combining the velocity measurements (Figure S4B) with the total flow cross section based on the designed dimensions (Device 1 in Figure S1C) of the device giving flow rates of 71±19 nL/s. The correspondence of the two types of measurements indicate that the flow is indeed taking place such that it fills up the space between the posts without overflowing.

Equivalent pressures applied to the device

The equivalent pressure exerted by the paper capillary pump is found to be 21 mBar by comparing the applied over-pressure necessary across a closed device to achieve the same flow velocities as for a closed device with a paper capillary pump (Figure S4B). The pressure exerted by the paper capillary pump exceeds the pressure due to the water pillar in the reservoir. The pressure generated in the reservoir depends on the height difference between the inlet and outlet ($\rho\, g\, \Delta h$ ~ 1 mBar/cm with ρ = 1000 kg/m^3 density of water, g = 9.8 m/s^2 gravitational acceleration, Δh height of water pillar). The tested volumes, 30 µL, 40 µL and 60 µL, correspond to heights of 4.2 mm, 5.6 mm and 8.4 mm of sample respectively in the reservoir (inner diameter 3mm) giving hydrostatic pressures of 0.4 mBar, 0.6 mBar and 0.8 mBar which is much less than the involved estimated negative pressures exerted by the capillary paper pump pulling the sample. The capillary pumping effect of the paper therefore dominates the flow and the fluid is predominantly pulled through the device.

Flow resistance

Flow resistance for the closed devices is estimated based on the relationship

$$Q_{pump}^{closed} = \frac{\Delta P_{pump}}{R_{load}^{closed}}$$

where R is the fluidic resistance, Q is the volumetric flow rate and ΔP is the applied pressure difference across the device. From figure S4B we obtain $R^{closed} = 30\ 10^{12}$ kgs^{-1}m^{-4}.

The flow resistance of the open device is expected to be slightly lower than that for the closed device. It is calculated below based on figure S5.

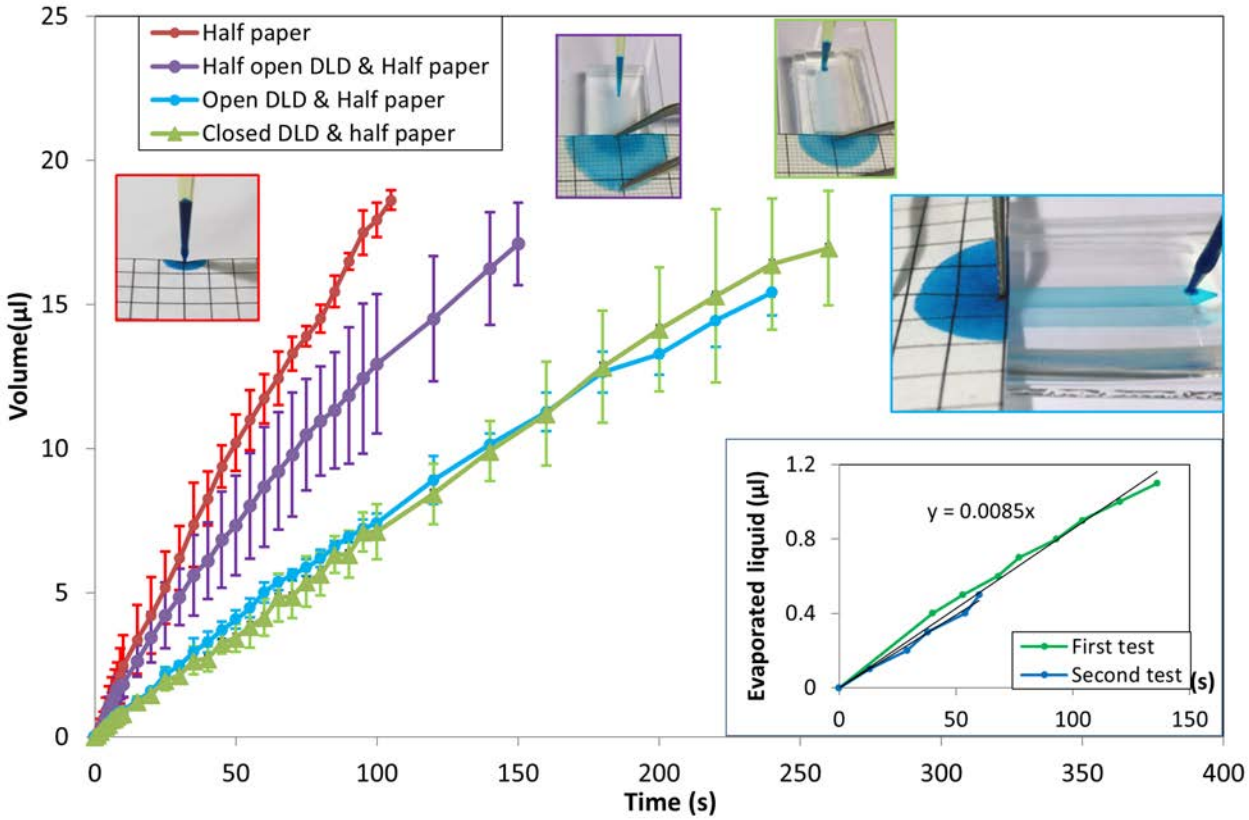

Figure S5. *Liquid flows versus time corrected for evaporation. The liquid is 0.5% food coloring diluted in deionized water. The graph shows four cases. From the left to the right we have: liquid added at the edge of a paper (half paper), open DLD device of length 10 mm (half device) connected to paper, open DLD of length 20 mm (whole device) connected to paper, closed DLD of length 20 mm (whole device) connected to paper. To be able to easily judge the extent of the drops on the paper, a grid pattern is printed on the paper using a standard laser writer. The inset shows the accumulated evaporated liquid from a filled device (device 1). From this graph we can conclude that the evaporation rate from the device is 8.5 nL per second.*

Characterization of the paper capillary pump

The paper capillary pump can be treated as a battery with an internal resistance and an internal negative pressure or, in analogy to electronics, a hydromotive force. To estimate the internal resistance and the hydromotive force the following system of equations (number 1 to 4) are considered. Note that we will obtain an estimate of the flow resistance of the open device from these calculations.

$$\begin{cases} Q_{paper} = \dfrac{\Delta P_{internal}}{R_{internal}} \\ Q_{paper}^{openHALF} = \dfrac{\Delta P_{internal}}{\frac{1}{2}R_{load}^{open} + R_{internal}} \\ Q_{paper}^{open} = \dfrac{\Delta P_{internal}}{R_{load}^{open} + R_{internal}} \\ Q_{paper}^{closed} = \dfrac{\Delta P_{internal}}{R_{load}^{closed} + R_{internal}} \end{cases}$$

We first calculate the internal resistance of the paper by combining equations 1 and 4 above to eliminate the internal pressure (hydromotive force).

$$R_{internal} = \frac{\Delta P_{pump}}{Q_{pump}^{closed}} \frac{Q_{paper}^{closed}}{Q_{paper} - Q_{paper}^{closed}}$$

Numerical data is extracted from Figures S4 (for the pump driven flow) and S5 (for the paper capillary pump driven flow) based on the initial flow rates for each case and combined with the flow resistance of the closed device as calculated above.

$$\Delta P_{pump} = 21 mBar$$
$$Q_{pump}^{closed} = 71 nL s^{-1}$$
$$Q_{paper} = 198 nL s^{-1}$$
$$Q_{paper}^{closed} = 71 nL s^{-1}$$
$$\Rightarrow R_{internal} = 16.5 \cdot 10^{12} kg s^{-1} m^{-4}$$

The hydromotive force is now calculated by using the number of the flow rate of the paper without any device (“Half paper”) in fig S5 combined with equation 1 above.

$$Q_{paper} = 198 nL s^{-1}$$
$$\Rightarrow \Delta P_{internal} = 32 mBar$$

Plugging the results above into equation 3 above, the flow resistance of the open device.

$$Q_{paper}^{open} = 80 nL s^{-1}$$
$$\Rightarrow R_{load}^{open} = 23.1 \cdot 10^{12} kg s^{-1} m^{-4}$$

Finally, as a simple control the flow rate of the device cut in half is estimated based on equation 2 above.

$$Q_{paper}^{openHALF*} = 113 nLs^{-1}$$

The value is lower but still consistent with the value obtained by measuring the initial slope of the corresponding curve in figure S5.

$$Q_{paper}^{openHALF} = 157 nLs^{-1}$$

Evaporation

To obtain rough estimates of the evaporation rates we measured the evaporation rates for different cases by using a precision balance (Ohaus Corp. Pine Brook, NJ USA, model Pioneer PA114C, minimal readout 1 µg).

An evaporation of 8 nL/s from the device can be compared to the typical flow rate through the device of 65 nL/s. Roughly 12% of the sample is thus evaporated from the device.

Due to nonuniform wetting and possible variations in the lab environment during the course of the experiments, the evaporation rates should be considered rough estimates to give a perspective of the relationship between the evaporation rate and the volumetric throughput in the devices.

The lab environment had a 60±5% RH and room temperature of 21°±1° C.

Biological samples

The size distributions of the biological samples used were determined by measurement in optical micrographs using ImageJ (Figure S6). The results are summarized in the following table.

Sample type	*Dimensions ± std dev*	*Shape*
MCF7 (cancer cell line)	17.3±2.1 µm	spherical
White blood cell	12.2±0.9 µm	spherical
Red blood cell	2.2±0.5 µm 7.8±0.6 µm	biconcave
Trypanosome cyclops	2.5±0.5 µm 12.8±3.3 µm	ribbon-like

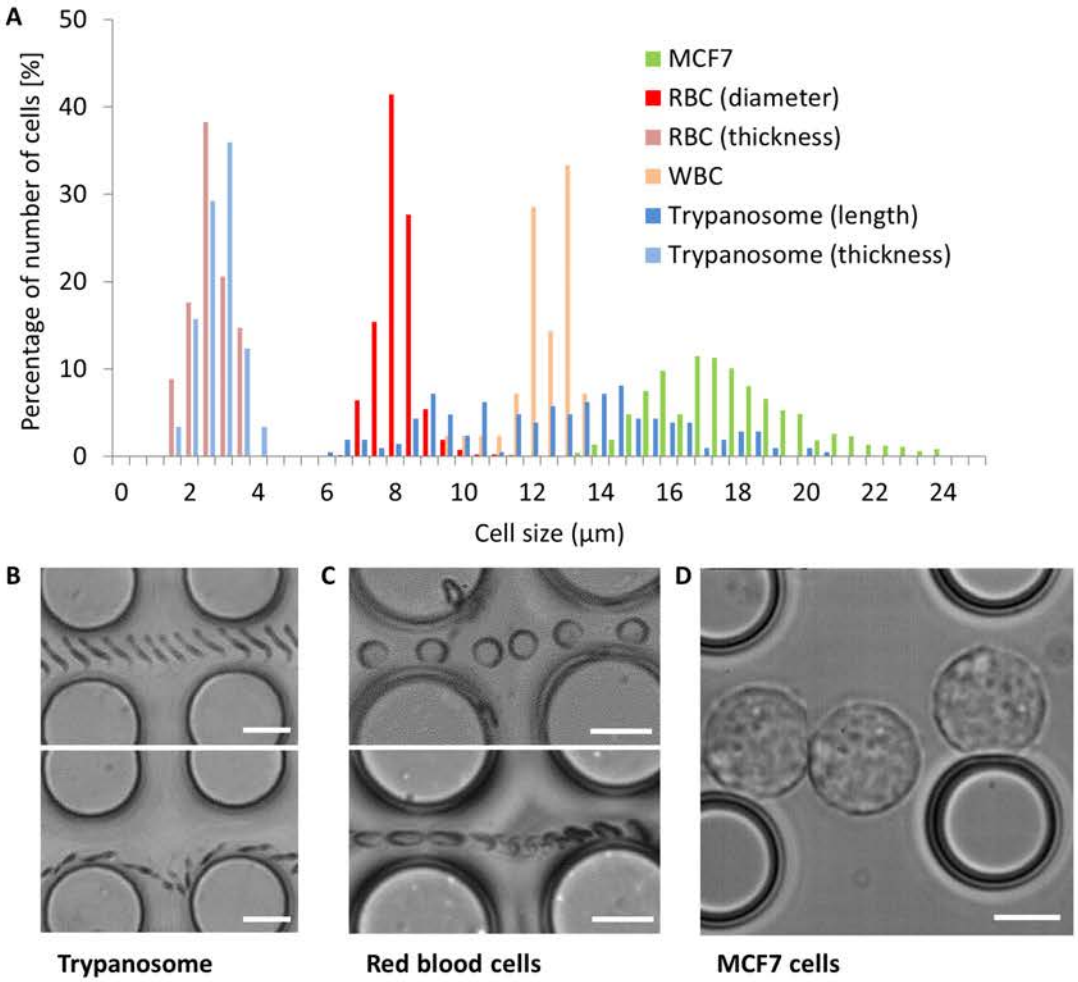

Figure S6*. Size distribution of biological samples based on measurements in optical micrographs. (A) Histograms of size distributions. For the spherical cells (MCF7 and WBC) one number gives the relevant size (diameter). Red blood cells and the parasites are described by two numbers (thickness and overall diameter or length). (B) & (C) Optical micrographs of the non-spherical cells exhibiting different orientations depending on device depth (9 µm and 24 µm) (top images shallow device and bottom images deep device) (D) Optical micrograph of spherical MCF7 cells. All scale bars 10 µm.*